Deformation bands in porous sandstones

their microstructure and petrophysical properties

Anita Torabi

Dissertation for the degree Philosophiae Doctor (PhD)

Department of Earth Science

University of Bergen

December 2007

Contents

Preface

The work presented in this dissertation was carried out in my PhD project. The project started in April 2005 at the Centre for Integrated Petroleum Research (CIPR), Department of Earth Science; University of Bergen (UiB). My PhD project has been a part of the "Fault Facies" project at CIPR. The Fault Facies project is a multi-disciplinary petroleum research project which aims to improve the implementation of faults in 3D geological reservoir models. The project has several different themes, one of which is focused on the micro-scale deformation structures known as deformation bands, which form during the process of fault initiation and also damage-zone development. This theme was developed in my PhD project, where the main concern was to increase our understanding of the microstructure and petrophysical properties of deformation bands and to investigate their effect on petrophysical characteristics of sandstone reservoirs.

This dissertation comprises four separate and complementary parts:

Part one (Introduction): This part describes the "state of the art" for deformation bands and their development, states the objectives of the research I conducted , and describes the relation between the four scientific papers that make up the main body of the thesis.

Part two (papers): The second part, which is the main outcome of my study, is a collection of four research papers, of which the first has already been published, and the second has been accepted for publication and the third is in review in an international journal. The fourth paper will soon be submitted.

The four papers included are:

Paper 1: Torabi A., Braathen, A., Cuisiat, F., and Fossen, H., 2007. Shear zones in porous sand: Insights from ring-shear experiments and naturally deformed sandstones. Tectonophysics, 437, 37-50.

This paper presents an analysis of analogue experimental modeling of shear zones based on original ring-shear experiments. It includes microscopic study of both experimental shear zones and natural deformation bands. The result of this study was also presented in Petroleum Geoscience Collaboration Conference, 24th -25th October 2006, The Geological Society, Burlington House, London.

Paper 2: Rotevatn, A., Torabi, A., Fossen, H., and Braathen, A., 2007. Slipped deformation bands: a new type of cataclastic deformation bands in Western Sinai, Suez Rift, Egypt. Accepted, Journal of Structural Geology.
The second paper describes a new type of cataclastic deformation band. This study reports original field outcrop study, optical microscopy and laboratory measurements.

Paper 3: Torabi, A., Fossen, H., and Alaei, B., 2007. Application of spatial correlation functions in permeability estimation of small-scale deformation bands in porous rocks. In review, Journal of Geophysical Research (Solid Earth).

Paper 4: Torabi, A., and Fossen, H., 2007. Spatial variation of microstructure and petrophysical properties of deformation bands. To be submitted to Journal of Structural Geology.
The third and the fourth papers comprise a detailed study of the microstructure of all types of deformation bands and an estimation of their petrophysical properties using an image processing method developed through this study. These works were presented in Winter Conference, 8^{th} -10^{th} January 2007, Stavanger, Organized by Geological Society of Norway, and also in StatoilHydro International Student Conference, 9^{th} – 13^{th} October 2007, StatoilHydro Research Center, Trondheim, Norway.

Part three (Synthesis): This part provides a synthesis of the results obtained at different parts of the study. It includes a brief discussion, and also addresses limitations of the different approaches applied in the conducted research. Some suggestions for future work are also included in this part.

Part four (Appendix): The last part contains the MATLAB program that was written to calculate the one- and two-point spatial correlation functions and specific surface area of the pore-grain interface from backscatter images of faulted sandstones.

Anita Torabi
December, 2007

Acknowledgements

My PhD project was a part of a larger CIPR research initiative called “Fault Facies” which was financed by the Norwegian Research Council (NRC), Statoil (now StatoilHydro) and Conoco-Philips. I would like to express my gratitude to all of my supervisors: Alvar Braathen for his encouragement and scientific discussions, and Arne Skauge, William Helland-Hansen and Fabrice Cuisiat for their support and useful comments. I would especially like to thank Haakon Fossen for his continuous guidance and generosity. His motivating comments and inspiration was crucial during my PhD project. I would also like to thank Egil Sev. Erichsen for his assistance with the Scanning Electrone Microscope. Jan Tveranger is acknowledged for sharing his knowledge and experience. I would like to thank Tore Skar for good collaboration during working at CIPR and also for his encouragement. Walter Wheeler is also appreciated for reviewing the introduction and synthesis parts of this dissertation. I would like to take the opportunity to express my appreciation to the administrations at the Earth Science Department and CIPR. Special thanks to Irene Huse who was always helpful when, in several crucial moments in my study, I was beset with computer-related problems. I am grateful to many friends and colleagues. I am indebted to my husband Behzad Alaei who has always been supportive and sympathetic and to my two lovely and intelligent children, my son Armin and my daughter Arezo, who were supportive and patient enough to tolerate the hard life of having a PhD student as mother. They sometimes participated in the scientific discussions at home and now after almost 3 years, they know these tiny, neat phenomena known as deformation bands very well. I would like to dedicate my thesis to my family for their love and support.

Abstract

Deformation bands are commonly thin tabular zones of crushed or reorganized grains that form in highly porous rocks and sediments. Unlike a fault, typically the slip is negligible in deformation bands. In this dissertation the microstructure and petrophysical properties of deformation bands have been investigated through microscopy and numerical analysis of experimental and natural examples. The experimental work consists of a series of ring-shear experiments performed on porous sand at 5 and 20 MPa normal stresses and followed by microscopic examination of thin sections from the sheared samples. The results of the ring-shear experiments and comparison of them to natural deformation bands reveals that burial depth (level of normal stress in the experiments) and the amount of shear displacement during deformation are the two significant factors influencing the mode in which grains break and the type of shear zone that forms. Two end-member types of experimental shear zones were identified: (a) Shear zones with diffuse boundaries, which formed at low levels of normal stress and/or shear displacement; and (b) Shear zones with sharp boundaries, which formed at higher levels of normal stress and/or shear displacement. Our interpretation is that with increasing burial depth (approximately more than one kilometer, simulated in the experiments by higher levels of normal stress), the predominant mode of grain fracturing changes from flaking to splitting; which facilitates the formation of sharp-boundary shear zones. This change to grain splitting increases the power law dimension of the grain size distribution (D is about 1.5 in sharp boundary shear zones). Based on our observations, initial grain size has no influence in the deformation behavior of the sand at 5 MPa normal stresses.

A new type of cataclastic deformation band is described through outcrop and microscopic studies; here termed a "slipped deformation band". Whereas previously-reported cataclastic deformation bands are characterized by strain hardening, these new bands feature a central slip surface, which indicates late strain softening. They lack the characteristic compaction envelop, and are typified by higher porosity and lower permeability than previously-described cataclastic deformation bands. Intense background fracturing of the host rock and significant initial porosity are considered to be important in creating these newly-discovered deformation bands.

In a related study, we investigate, for millimeter- wide deformation bands, the scale limitation inherent in laboratory measurements of porosity and permeability. The scale

limitations imposed by the deformation band relative to the physical sample size motivated us to develop a new method for determining porosity and permeability based on image processing. While plug measurements measure the effective permeability across a 25.4 mm (1 inch) long sample, which includes both host rock and deformation band, the method presented here provides a means to estimate porosity and permeability of deformation band on microscale. This method utilizes low-order (one- and two-orders) spatial correlation functions to analyze high-resolution, high-magnification backscatter images, to estimate the porosity and specific surface area of the pore-grain interface in the deformed sandstones. Further, this work demonstrates the use of a modified version of the Kozeny-Carmen relation to calculate permeability by using porosity and specific surface area obtained through the image processing. The result shows that permeability difference between the band and the host rock is up to four orders of magnitude. Moreover, the porosities and permeabilities estimated from image processing are lower than those obtained from their plug measurements; hence the traditional laboratory measurements have been overestimating permeability because of the previously-unrecognized scale problem. In addition, the image processing results clearly show that, as a result of microstructural variation, both porosity and permeability vary along the length of individual deformation bands, with permeability variations of up to two orders of magnitude. Such petrophysical variations are found in several types of deformation bands (disaggregation, cataclastic and dissolution bands), but the range depends on the deformation mechanisms, in particular on the degree of (i) cataclasis, (ii) dissolution in cataclastic and dissolution bands, and (iii) on the phyllosilicate content in disaggregation bands. This microscopic anisotropy in the petrophysical properties of deformation bands opens up a new and fruitful area for further research. Our results show that for phyllosilicate bands the band thickness is related to the phyllosilicate content, whereas for cataclastic bands no apparent correlation was found between thickness and intensity of cataclasis.

Introduction

Sedimentary rocks, whether they are water aquifer or petroleum reservoirs are characterized by features which affect the fluid flow. The faulting of clastic rocks can induce large- and small-scale heterogeneities in the spatial distribution of petrophysical characteristics, particularly porosity and permeability. Enhanced understanding of the structure and the petrophysical properties of fault zones in comparison to the surrounding undeformed host rock is essential when efforts are made to predict fluid flow through faulted reservoirs.

Many workers have provided a theoretical foundation for understanding the movement of fluids, especially hydrocarbons, in the subsurface (e.g. Hubbert, 1953; Berg, 1975; Schowalter, 1979; England, 1987; Watts, 1987). However, applying such studies to the movement of hydrocarbons within faulted reservoirs has been limited by the absence of detailed data on the petrophysical properties of fault rocks (e.g. porosity and permeability), as well as the distribution of fault-related deformation structures (e.g. Fisher et al., 2001). Recent publications have provided quantitative data on the petrophysical properties of faults and their associated localized microstructures, known as deformation bands (e.g. Antonellini and Aydin, 1994; Fisher and Knipe, 1998; Gibson, 1998, Fisher and Knipe, 2001; Hesthammer and Fossen, 2001; Ogilvie and Glover, 2001; Shipton, et al., 2002), the distribution of fault related structures (e.g. Allan, 1989; Knipe, 1997; Yielding et al., 1997; Shipton et al., 2001), as well as the fault zone structures in both macro- and microscale (e.g. Cowie and Scholz, 1992; Gibson, 1994; Peacock and Sanderson, 1994; McGrath and Davison, 1995; Knipe et al., 1997; Fossen et al., 2007).

Although such data are required as input to reservoir simulators, large uncertainties exist in the detail of the associated structures in the fault zones and absolute values of properties; these uncertainties ultimately have large influence on the predicted fluid flow. The main aim of the studies in this dissertation is to improve our knowledge of deformation bands and their petrophysical properties such as porosity and permeability. As a complete review of the existing literature is provided through the enclosed papers, the following section is a brief overview of the state of the art for the studied topic.

Deformation bands and their petrophysical properties

Deformation bands are tabular, thin structures, which form at the onset of strain localization in porous rocks (e.g. Rudnicki and Rice, 1975, Bésuelle, 2001a; Klein et al., 2001; Rudnicki, 2002; Olsson et al., 2002, Rudnicki, 2004; Schultz and Siddharthan, 2005, Aydin et al., 2006; Fossen et al., 2007, Holcomb et al., 2007, Fig. 1) . They are preferentially oriented with respect to the stress field (Bésuelle, 2001). Deformation bands are different from faults and fractures in that they do not feature a discrete fracture or slip surface (e.g. Fossen et al., 2007).

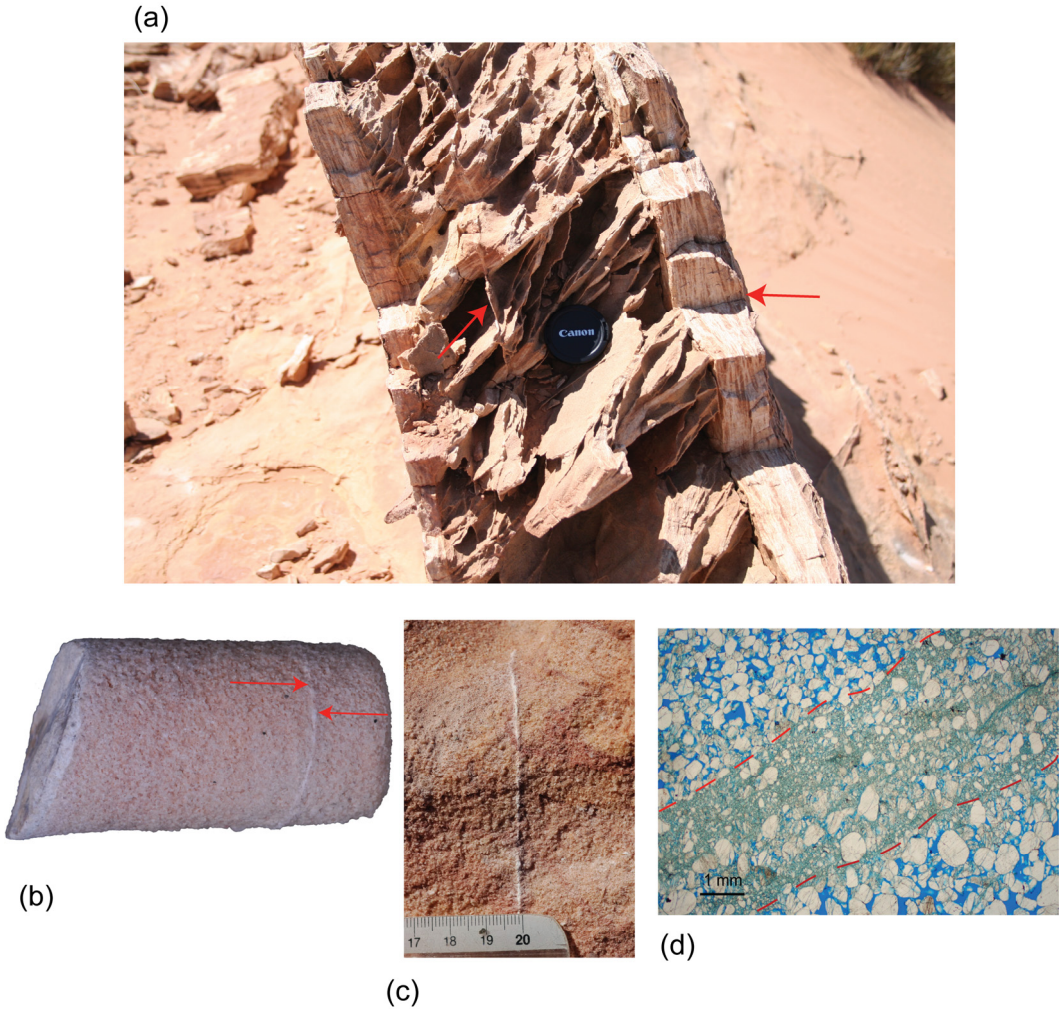

Fig.1. Deformation bands at different scales: (a) Deformation bands(marked by the arrows), outcrop photo (lens-cap for scale) ; (b) A millimeter wide deformation band (marked by the arrows) in a cylindrical plug of sandstone (length of the plug is 25.4 mm/ 1 inch); (c) A millimeter wide deformation band in a hand sample, the scale bar is in centimeters (d) photomicrograph of a deformation band outlined with red dashed lines, quartz grains are white, epoxy saturating the pore space is blue.

Field and laboratory observation show that they are not necessarily associated with a dilational strain. Very often they show porosity reduction (Bésuelle, 2001). Deformation bands range from compactional through simple shear to dilational (e.g. Anttonellini and Aydin, 1994; Antonelli et al., 1994; Mollema and Antonellini, 1996, Cashman and Cashman, 2000; Du Bernard et al., 2002) and involve different deformation mechanisms including particulate (granular) flow, cataclasis and dissolution (e.g. Gibson, 1994; Rawling and Goodwin, 2003; Fossen et al, 2007, Fig. 2). Disaggregation bands form as result of granular flow and involve rolling, sliding and reorganization of the sand grains in sand or sandstones at shallow depth or low effective stress (e. g. Rawling and Goodwin, 2003). Disaggregation bands (Fig. 2a) do not affect the petrophysical properties of the deformed sandstone significantly. Cataclastic deformation bands (Fig. 2c) are characterized by grain abrasion, crushing or cataclasis and can reduce porosity and permeability of deformed sandstones significantly (Antonellini and Aydin, 1994). Dissolution and cementation bands form where dissolution or cementation is dominant (Fig. 2d). Dissolution and quartz cementation have been suggested as an explanation for poor reservoir performance in North Sea reservoirs located at >3 km depth (Hesthammer et al., 2002).

Typical deformation bands such as those first reported by Aydin (1978) in Utah, are about a millimeter thick, several meters to hundreds of meters in length and have maximum displacements in the range of several millimeters to several centimeters. These bands consist of two zones, namely inner zone and outer zone. The inner zone comprises a zone of fractured and crushed grains, whereas the deformation in outer zone was restricted to reorganization of the grains and pore collapse (Aydin, 1978; Aydin and Johnson, 1978).

The Localization and development of deformation bands and the evolution of their permeability structure have been investigated through experimental work (e.g. Mair et al., 2000; Main et al., 2001; Lothe et al., 2002; Ngwenya, et al., 2003). In the course of deformation mechanism in porous sand and sandstone, controlling factors have been conveniently isolated and studied in the laboratory. Such studies have attracted significant attention from geologists, rock- and soil-mechanics engineers, and geophysicists (Mandl et al., 1977; Zhu and Wong, 1997; Zhang and Tullis, 1998; Main et al., 2001; Mair et al., 2000; 2002; Sperrevik et al., 2002; Lothe et al., 2002; Garga and Sendano, 2002; Clausen and Gabrielsen, 2002; Kjelstad et al., 2002; Ngwenya et al., 2003; Agung et al., 2004; Sassa et al., 2004). Numerical modeling of deformation bands

has also provided valuable insights (e.g. Antonellini et al., 1995; Wang et al., 2001; Borja, 2003; Narteau and Main, 2003; Schultz & Balasko, 2003; Okubo and Schultz, 2005).

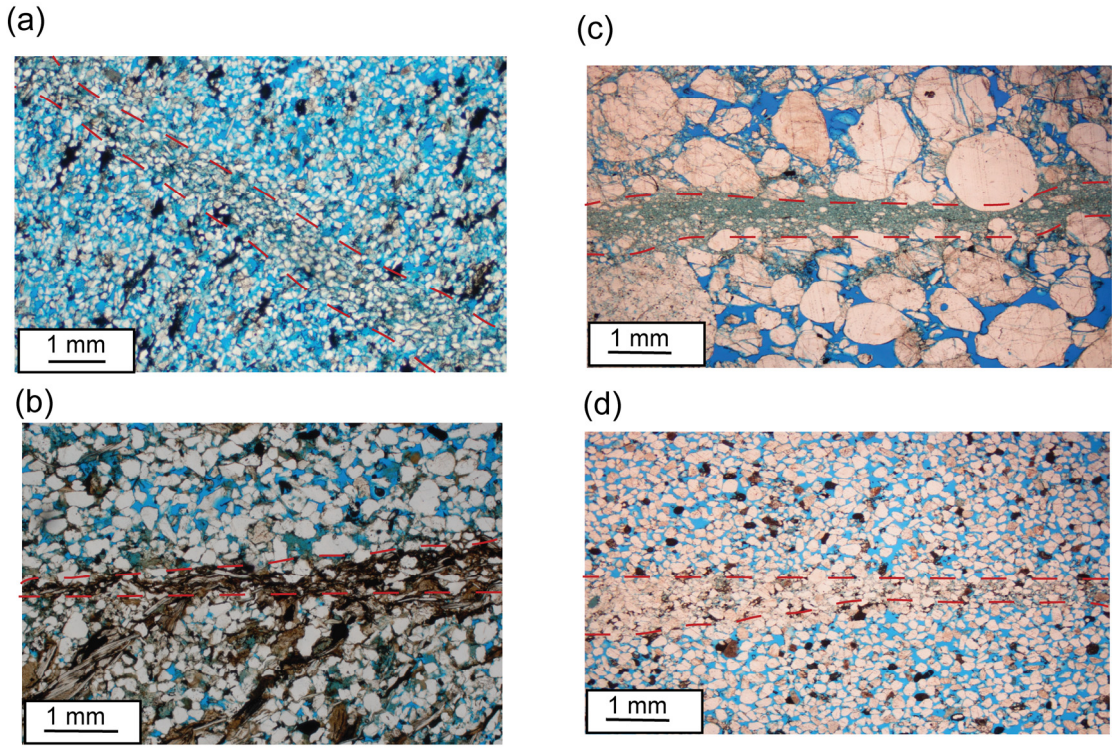

Fig.2. Examples of deformation bands formed as results of different deformation mechanisms; (a) A disaggregation band from Gullfaks field, North Sea(b) A phyllosilicate band from Huldra field, North Sea (c)A cataclastic band from Sinai, Egypt (d) A dissolution band from San Rafael Desert,Utah.

Several publications address the effects of the small-scale geological features on large-scale permeability of the reservoirs (e.g. Durlofsky, 1992; Jourde, 2002; Sternlof et al., 2004). For more than two decades, much attention has been devoted to the petrophysical properties of deformation bands, in particular permeability reduction caused by the presence of deformation bands in faulted sandstones (Pitman, 1981; Jamison and Streans, 1982; Antonellini and Aydin, 1994; Knipe et al., 1997; Gibson, 1998; Fisher and Knipe, 2001; Ogilvie and Glover, 2001; Shipton et al., 2002; Sternlof et al., 2004). Individual cataclastic deformation bands in Utah are reported to reduce the porosity of the host sandstone by one order of magnitude and the permeability by three orders of magnitude (Antonellini and Aydin, 1994).

Phyllosilicate bands (Fig. 2b), which form by granular flow in sandstones containing more than 10-15% phyllosilicate, involve up to several orders of reduction in permeability according to plug measurements reported by Fisher and Knipe (2001). However, the dispersion in the reported porosity and permeability data for deformation bands is noticeable. Moreover, spatial variations in porosity and permeability, related to microstructural variations along individual deformation bands, have been given little or no attention in the literature (cf. Fossen and Bale, 2007).

In addition, most of the published porosity and permeability data for deformation bands are from either mini-permeameter or plug measurements. A central question is whether these data are representative of the permeability effects of millimeter wide deformation bands? What kinds of uncertainties are associated with these methods? There has been significant progress in numerical permeability models for sandstone reservoirs, one could ask whether existing image processing based methods typically applied to undeformed sandstones (e.g. Ehrlich et al., 1984; Wissler, 1987; Koplik et al., 1984; Doyen, 1988; Blair et al., 1996, Bakke and Øren, 1997; Keehm et al., 2004; 2006; White et al., 2006) could be used to estimate the porosity and permeability of deformation bands?

Objectives of this study

The prediction of fluid flow paths in deformed porous sandstone requires more accurate geological models of deformation band morphology, and their evolution. The studies collected in this dissertation share the common aim of increasing our understanding of the detailed microstructure and petrophysical properties of deformation bands with special reference to deformation bands formed in extensional geological settings, in particular rift related structures similar to the North Sea. In order to achieve this goal a three-part workflow was defined.

1- Analogue modeling of deformation bands by ring-shear experiments (Paper 1). In the ring-shear project, we aimed to investigate the initiation and development of shear zones in highly porous sand at different stress levels. The effect of grain size on deformation process was also studied. Fundamental for this study was the creation of shear zones which are similar to natural deformation bands formed at shallow to medium burial depth.

2- Outcrop study; an outcome of this work was establishing a database on thin sections of different types of deformation bands. Our database involves examples from Corsica (France), Sinai (Egypt), Utah (USA). The main focus was to present a new type of deformation band, first observed by us during the field and laboratory works on samples from Sinai, Egypt (Paper 2). These bands are distinct from other deformation bands in our database. The work examines the microstructure and petrophysical properties of this new band type and discusses mechanisms and causes for their formation.

3- Numerical analysis of the petrophysical properties of deformation bands and their host rock, such as porosity and permeability (Papers 3 and 4); the main concern for this part was to find a reasonably accurate method to estimate the porosity and permeability of deformation bands. Furthermore we sought to explain the wide dispersion in the published petrophysical properties of deformation bands. Examples of different types of deformation bands from localities around the world were examined using optical microscopy, Secondary Electron Microscope and image processing.

References

Agung, M. W., Sassa, K., Fukuoka, H., Wang, G., 2004. Evolution of shear-zone structure in undrained ring-shear tests. Landslides 1, 101-112.

Allan, U. S., 1989. Model for hydrocarbon migration and entrapment within faulted structures. AAPG Bulletin, 73, 803-811.

Antonellini, M. and Aydin, A., 1994. Effect of faulting on fluid flow in porous sandstones: petrophysical properties, AAPG Bulletin, 78, 355-377.

Antonellini, M.A., Aydin, A. & Pollard, D. D., 1994. Microstructure of deformation bands in porous sandstones at Arches National Park, Utah. Journal of Structural Geology, 16, 941–959.

Antonellini, M. and Pollard, D., 1995. Distinct element modelling of deformation bands in sandstone, Journal of Structural Geology, 17, 8, 1165-1182.

Aydin, A., 1978. Small faults formed as deformation bands in sandstone. Pure and applied Geophysics 116: 913-913.

Aydin, A., Johnson, A. M., 1978. Development of faults as zones of deformation bands and as slip surfaces in sandstone. PAGEOPH 116.

Aydin, A., Borja, R. I. and Eichhubl, P., 2006.Geological and Mathematical framework for failure modes in granular rock. Journal of Structural Geology, 28, 83-98.

Bakke, S. and Øren, P. E., 1997. 3-D Pore-scale modelling of sandstones and flow simulations in the pore networks, SPE 35479, 2.

Berg, R. R. (1975). Capillary entry pressure in stratigraphic traps. AAPG Bulletin, 59, 939-956.

Blair, S. C., Berge, P. A., and Berryman, J. G., 1996. Using two-point correlation functions to characterize microgeometry and estimate permeabilities of sandstones and porous glass, J. Geophys. Res., 101(B9), 20359-20375.

Borja, R. I., 2003. Computational modelling of deformation bands in granular media. II. Numerical Simulatiions, Comput. Methods Appl. Mech. Engreg. 193, 2699-2718.

Bésuelle, 2001. Compacting and dilating shear bands in porous rocks: Theoretical and experimental conditions, Journal of Geophysical Research, Vol. 106, No.87, P. 13,435-13,442.

Cashman, S. & Cashman, K., 2000. Cataclasis and deformation-band formation in unconsolidated marine terrace sand, Humboldt County, California. Geology,28, 111–114.

Clausen, J. A., Gabrielsen, R. H., 2002. Parameters that control the development of clay smear at low stress states: an experimental study using ring-shear apparatus. Journal of Structural Geology 24(10), 1569-1586.

Cowie, P.A. & Scholz, C.H., 1992. Displacement–length scaling relationship for faults: data synthesis and analysis. Journal of Structural Geology, 14, 1149–1156.

Doyen, P. M., 1988. Permeability, conductivity, and pore geometry of sandstone, J. Geophys. Res., 93, 7729-7740.

Du Bernard, X. D., Eichhubl, P., and Aydin, A., 2002. Dilation bands: A new form of localized failure in granular media, Geophysical Research Letters 29(24), 2176.

Ehrlich R., Kennedy, S. K., Crabtree, S. J. and Cannon, R. L., 1984. Petrographic image anlysis: I. Analysis of reservoir pore complexes, Journal of Sedimentary Petrology, 54, 1515-1522.

England, W.A., MacKenzie, A.S., Mann, D.M., Quigley, T.M., 1987. The movement and entrapment of petroleum fluids in the subsurface. Journal of the Geological Society, 144, 327– 347.

Fisher, Q. J., & Knipe, R. J., 1998. Microstructural controls on the petrophysical properties of fault rocks. In G. Jones, Q. J. Fisher & R. J. Knipe, Faulting and fault

sealing in hydrocarbon reservoirs. Geological Society of London Special Publications 147, 117-135, London; The Geological Society.

Fisher, Q.J., Harris, S. D., McAllister, E., Knipe, R. J., Bolton, A. J., 2001, Marine and Petroleum Geology, 18, 251-257.

Fisher, Q. J. and Knipe, R. J., 2001. The permeability of faults within siliciclastic petroleum reservoirs of the North Sea and Norwegian Continental Shelf, Marine and Petroleum Geology, 18, 1063-1081.

Fossen, H., Schultz, R. A., Shipton, Z., Mair, K., 2007. Deformation bands in sandstone-a review. Journal of the Geological Society, London, 164, 4, 755-769.

Fossen, H & Bale, A. 2007: Deformation bands and their influence on fluid flow. AAPG Bulletin 91, 1685-1700.

Gibson, R.G. 1994. Fault-zone seals in siliciclastic strata of the Columbus Basin, offshore Trinidad. AAPG Bulletin, 78, 1372–1385.

Gibson, R.G. 1998. Physical character and fluid-flow properties of sandstone derived fault zones. In: Coward, M.P., Johnson, H. & Daltaban, T.S. (eds) Structural Geology in Reservoir Characterization. Geological Society, London, Special Publications, 127, 83–97.

Hesthammer, J. and Fossen, H., 2001. Structural core analysis from the Gullfaks area, northern North Sea, Marine and Petroleum Geology 18, 411-439.

Hesthammer, J., Bjorkum, P. A., Watts, L., 2002. The effect of temperature on sealing capacity of faults in sandstone reservoirs: Examples from the Gullfaks and Gullfaks Sør fields, North Sea, AAPG Bulletin.

Holcomb, D., J. W., Rudnicki, K. A., Issen, K., Sternlof, 2007. Compaction localization in the Earth and laboratory: state of the research and research directions, Acta Geotechnica, 2, 1-15.

Hubbert, M. K. (1953). Entrapment of petroleum under hydrodynamic conditions. AAPG Bulletin, 37, 1954-2026.

Jamison, W.R. & Stearns, D.W. 1982. Tectonic deformation of Wingate Sandstone, Colorado National Monument. AAPG Bulletin, 66, 2584–2608.

Jourde, H., Flodin, E. A., Aydin, A., Durlofsky, L. J., and Wen, X-H., 2002. Computing permeability of fault zones in eolian sandstone from outcrop measurements, AAPG Bulletin, 86(7), 1187-1200.

Keehm, Y., Mukerji, T., Nur, A., 2004. Permeability prediction from thin sections: 3D reconstruction and Lttice-Boltzmann flow simulation, Geophys. Res. Let., 31, L04606.

Keehm, Y., Sternlof, K., Mukerji, T., 2006. Computational estimation of compaction band permeability in sandstone, Geosciences Journal, 10, 4, 499-505.

Kjelstad, A., Chuhan, F., Høeg, K., Bjørlykke, K., 2002. Cataclastic shear band formation in sands at high stresses: An analogue experimental model and its relevance for faults in sedimentary basins. PhD Thesis, University of Oslo.

Klein, E., P., Baud, T., Reuschle and T-f., Wong, 2001. Mechanicl behaviour and failure mode of Bentheim Sandstone under triaxial compression, Phys. Chem., Earth (A), Vol. 26, NO. 1-2, pp. 21-25

Knipe, R.J., Fisher, Q.J. & Clennell, M.R. et al. 1997. Fault seal analysis: successful methodologies, application and future directions. In: Møller-Pedersen, P. & Koestler, A.G. (eds) Hydrocarbon Seals: Importance for Exploration and Production. Norwegian Petroleum Society Special Publication, 7, 15–40.

Knipe, R. J., Fisher, Q. J., Jones, G., Clennell, M. B., Farmer, B., Kidd, B., McAllister, E., Porter, J. R., & White, E. A., 1997, Fault seal prediction methodologies, applications and successes. In P. Mùller-Pedersen, & A. G. Koestler (Eds.), Hydrocarbon seals Ð importance for exploration and production. Special Publication NPF, 7, 15-38, Amsterdam; Elsevier.

Koplik, J., Lin, C., Vermette, M., 1984. Conductivity and permeability from microgeometry, J. Appl. Phys., 56, 3127-3131.

Lothe, A. E., Bjørnevoll Hagen, N., Gabrielsen, R. H., Larsen, B.T., 2002. An experimental study of the texture of deformation bands: effects on porosity and permeability of sandstones. Petroleum Geoscience 8, 195-207.

Main, I., Mair, K., Kwon, O., Elphick, S., and Ngwenya, B., 2001. Experimental constraints on the mechanical and hydraulic properties of deformation bands in porous sandstones: a review. In: Holdsworth, R. E, Strachan, R. A., Magloughlin, J. F. and Knipe, R. J. (Eds). The Nature and Tectonic Significance of Fault Zone Weakening. Geological Society, London, Special Publication, 186, 43-63.

Mair, K., Marone, C., 1999. Friction of simulated fault gouge for a wide range of velocities. Journal of Geophysical Research 104(B12), 28,899-28,914.

Mair, K., Main, I. G. and Elphick, S. C., 2000. Sequential growth of deformation bands in the laboratory. Journal of Structural Geology 22, 25-42.

Mair, K., Frye, K. M., Marone, C., 2002. Influence of grain characteristics on the frictioin of granular shear zones. Journal of Geophysical Research 107(B10).

Mandl, G., de Jong L. N., Maltha, A., 1977. Shear zones in granular material. Rock Mechanics. 9, 95-144.

Marone, C., Scholz, C. H, 1989. Particle-size distribution and microstructures within simulated fault gouge. Journal of Structural Geology 11(7), 799-814.

McGrath, A., & Davison, I., 1995. Damage zone geometry around faulttips. Journal of Structural Geology, 17, 1011-1024.

Mollema, P.N. & Antonellini, M.A. 1996. Compaction bands: a structural analogue for anti-mode I cracks in aeolian sandstone. Tectonophysics, 267, 209–228.

Ngwenya, B. T., O. Kwon, et al. (2003). "Permeability evolution during progressive development of deformation bands in porous sandstones. Journal of Geophysical Research 108(B7): 2343 10. 1029/2002JB001854.

Ogilvie, S. R., Glover, Paul, W. J, 2001. The petrophysical properties of deformation bands in relation to their microsturcture. Earth and Planetary Science Letters, 193, 129-142.

Okubo, C. H., Schultz, R. A., 2005. Journal of the Geological Society, London, 162, 939-949.

Olsson, W. A., D. J., Holcomb, J. W. Rudnicki, 2002, Compaction loclization in porous sandstone: implication for reservoir mechanics, Oil & Gas science and Technology, Rev. IFP, Vol., 57, No. 5, pp. 591-599

Peacock, D. C. P., & Sanderson, D. J., 1994. Geometry and development of relay ramps in normal fault systems. American Association of Petroleum Geologists Bulletin, 78, 147-165.

Pittman, E. D., 1981. Effect of fault-related granulation on porosity and permeability of quartz sandstones, Simpson Group (Ordovician) Oklahoma, AAPG Bull., 65, 2381-2387.

Rawling, G. C., Goodwin, L. B., 2003. Cataclasis and particulate flow in faulted, poorly lithified sediments. Journal of Structural Geology 25(3), 317-331.

Rudnicki, J. W., J. R., Rice, 1975, Conditions for the localization of deformation in pressure-sensitive dilatant materials, J. Mech. Phys., Solids, 1975, Vol. 23, pp. 371-394

Rudnicki, J. W., 2002. Condition for compaction and shear bands in a transversely isotropic material, International Journal of Solids and Strcuctures, 39, pp. 3741-3756

Rudnicki, J. W., 2004. Shear and compaction band formation on an elliptic yield cap, Journal of Geophysical Research, Vol. 109

Sassa, K., Fukuoka, H., wang, G., Ishikawa, N., 2004. Undrained dynamic-loading ring-shear apparatus and its applicatiion to landslide dynamics. Lanslides 1, 7-19.

Schowalter, T. T. (1979). Mechanisms of secondary hydrocarbon migration and entrapment. AAPG Bulletin, 63, 723-760.

Schultz, R. A. and Balasko, C. M., 2003. Growth of deformation bands into echelon and ladder geometries, Geophysical Research Letters, 30, 2033.

Schultz, R. A., Siddharthan, R., 2005. A general framework for the occurrence and faulting of deformation bands in porous granular rocks, Tectonophysics, 411, 1-18.

Shipton, Z.K. & Cowie, P.A. 2001. Analysis of three-dimensional damage zone development over _m to km scale range in the high-porosity Navajo sandstone, Utah. Journal of Structural Geology, 23, 1825–1844.

Shipton, Z. K., Evans, J. P., Robeson, K. R., Forster, C: B., Snelgrove, S., 2002. Structural heterogeneity and permeability in eolian sandstone: Implications for subsurface modelling of faults. AAPG Bull. 86 (%), 863-883.

Sperrevik, S., Gillespie, P. A., Fisher, Q. J., Halvorsen, T., Knipe, R. J., 2002. Empirical estimation of fault rock properties. In: Koestler, A. G. and Hunsdale, R. (Eds). Hydrocarbon Seal Quantification. Norwegian Petroleum Society (NPF), Special Publication. 11,109-125.

Sternlof, K. R., Chapin, J. R., Pollard, D. D., and Durlofsky, L. J., 2004. Permeability effects of deformation band in arrays in sandstone. AAPG Bull., 88, 9, 1315-1329.

Watts, N. L. (1987). Theoretical aspects of cap-rock and fault seals for single and two phase hydrocarbon columns. Marine and Petroleum Geology, 18, 4, 274-307.

Wissler, T. M., 1987. Sandstone pore structure: A quantitative analysis of digital SEM images, PhD. thesis, Mass. Inst. of Technol., Cambridge.

White, J., A., Borja, R. I., Fredrich, J. T., 2006. Calculating the effective permeability of sandstone wit multiscale lattice Boltzmann/finite element simulations. Acta Geotechnica, 1, 195-209.

Yielding, G., Freeman, B., & Needham, D. T., 1997. Quantitative fault seal prediction. American Association of Petroleum Geologists Bulletin, 81, 897-917.

Zhang, S., Tullis, T. E., 1998. The effect of fault slip on permeability and permeability anisotropy in quartz gouge. Tectonophysics 295(1-2), 41-52.

Zhu, W., Wong, T., 1997. The transition from brittle faulting to cataclastic flow. Journal of Geophysical Research 102(B2), 3027-3041.

Synthesis

Synthesis

This dissertation contributes to our detailed understanding of the microstructure of deformation bands and their related petrophysical properties. The papers presented in this dissertation address deformation bands, their microstructure, and evolution; and how they affect porosity and permeability (petrophysical properties) in porous sandstones. Here I synthesize the papers, discussing the findings reported in the individual papers with respect to each other. Implementation of such studies to the geological and simulation models for reservoirs can provide more realistic models. The ultimate goal is improved understanding of hydrocarbon flow within faulted reservoirs.

Progress on deformation band microstructure

We have compared experimentally-produced shear zones that resemble deformation bands to natural deformation bands, acknowledging that the deformation process is to some extent different in the ring-shear experimental apparatus than in natural deformation bands (Paper 1). The key difference is that in the ring-shear experiments the displacement and strain rate are far larger than in the natural setting. One can say that larger displacements in the experimental shear zones make them more comparable to faults than deformation bands. However, utilizing the ring-shear apparatus for deformation of highly-porous sand in a condition similar to shallow to medium burial depth and having the constrained thickness of the sample to the space between the rings, makes our comparison reasonable. In another word, the experimental shear zones have similar thickness to the single natural deformation bands.

We have identified variation in microstructure across experimental shear zones which are comparable to that seen in natural deformation bands (Paper 1). This variation has been previously addressed by a number of workers (e.g. Aydin, 1978; Aydin and Johnson, 1978, 1983; Gabrielsen and Aarland, 1990; Davis, 1999; Agung, 2004). The thin section microscopy studies of experimental shear zones produced by the ring-shear apparatus revealed the presence of three layers: a top layer, a central shear zone and a bottom layer (Paper 1).

The experimental shear zones were classified into two groups, *diffuse boundary shear zones* and *sharp boundary shear zones.* Diffuse boundary shear zone formed at low levels of normal stress and/or shear displacement, whereas sharp boundary shear zone formed at high normal stress and/or at high shear displacements. The sharp

boundary shear zone has not been previously reported from ring-shear experiments performed on sand or sandstone. The sharp boundary shear zones consist of margins of crushed and compacted grains around a more crushed and compacted central part which shows maximum reduction in particle size and significant porosity decrease. These shear zones are similar in microstructure to the classic deformation bands reported by Aydin (1978), which also have a compacted outer layer, but in which the deformation mechanism is mainly pore collapse.

The significant parameter that controls the transition from diffuse to sharp boundary shear zone is the transition of the grain fracturing mode from dominant flaking (e.g. Rawling and Goodwin, 2003; Paper 1) to dominant splitting. The transition occurs as a result of increasing the level of stress in the ring shear (similar to increasing the confining pressure in nature). This shift results in an increase in the D value (the power dimension of the grain size distribution fit). D has a good inverse correlation with the degree of cataclasis and grain size reduction (Blenkinsop, 1991; An & Sammis, 1994). However, the D values are relatively low in the experimental sharp boundary shear zone (D reaches a maximum of 1.5), suggesting that they have not reached the steady state particle size distribution (D~2.58).

Study of the effect of grain size on the frictional behavior of sand in the ring-shear experiments indicates that initial grain size has no influence on the deformation behavior at 5 MPa normal stresses (Paper 1; Kjelstad et al., 2002). On the other hand, Mair et al (2002) based on experiments from 5 MPa to 40 MPa stress, showed that grain characteristics, such as grain size distribution and roughness, have a clear effect on the frictional behavior of granular shear zones. In our ring-shear experiments, we have not investigated the effect of grain characteristics on experiments at more than 5 MPa.

Visual inspection of the experimental shear zones revealed that diffuse boundary shear zones are wider than sharp boundary ones (Paper 1). This is in agreement with results from numerical study of strain localization in granular material by for example Alsaleh (2006) and Alshibli et al. (2006). These studies showed that shear band thickness was found to decrease with increasing confining pressure. However, we have also demonstrated (Paper 4) that in natural deformation bands under constant confining pressure at the scale of a single deformation band, there is no simple relationship between thickness of the cataclastic deformation band and the degree of cataclasis within the band. The degree of cataclasis which is a factor of strain localization varies within Cataclastic deformation bands. Other factors that influence the thickness of deformation

bands during localization, such as grain characteristics, mineralogy, and initial porosity, need to be further investigated by both experimental and numerical studies. Besides, the research presented here shows there is a direct relationship between the thickness of the bands and the proportion of phyllosilicate (Paper 4).

Several of our studies have examined the spatial variation of deformation band microstructure, a topic which has received little or no attention in the literature. In this light, it is of interest that we show that a single band can change in thickness and microstructure over a short (mm-scale) distance. The variation in microstructure of the band implies that there is spatial variation in its petrophysical properties; this will be discussed further in the next sections.

A new type of deformation band has also been introduced through outcrop (Sinai, Egypt) and microscopy studies; here termed a *slipped deformation band* (Paper 2). Slipped deformation bands, characterized by a central slip surface, are different from conventional deformation bands (e.g. Aydin, 1978; Davatzes & Aydin 2003, Shipton & Cowie 2003, Johnson & Fossen in press). There is no compaction zone around the central part of the band in the slipped deformation bands from Sinai, Egypt. Therefore, in the slipped bands, the transition from the mildly-fractured background (host) rock to the band is sharp. We termed these individual tiny deformation bands "slipped deformation bands" because they can accumulate abundant shear strain and exhibit a slip surface. It is unclear how they form, but one plausible explanation can be found by the cam-cap model (e.g. Rudnicki & Rice, 1975; Rudnicki, 2002; Schultz & Siddharthan, 2005, Fossen et al., 2007; Holcomb et al., 2007). The background fracturing was probably induced during initial compaction as a result of overburden pressure, after which the deformation bands formed in a condition near simple shear-compaction in the field to the right-hand side of the cam-cap (Paper 2). The condition for localization of these bands is uncertain, but the parameters such as initial grain size and porosity should be significant.

Image processing technique for estimation of porosity and permeability

While microstructural variations along as well as across deformation bands are easily studied under the microscope, their internal permeability structure is difficult to assess by means of classical methods (e.g. permeability obtained from mini-permeameter and laboratory plug measurements). Mini-permeameter and laboratory plug measurements directly measure porosity and permeability for a band together with

its less deformed surrounding, whereas by application of image processing method, we are able to isolate the properties of only deformation band.

We have developed an image processing-based method which is applied on high resolution and -magnification images of thin sections. The image processing method applies statistical approaches such as spatial correlation functions to obtain porosity and specific surface area of the pore-grain interface from backscatter images of sandstone. In this method, we are able to catch the irregularities of the pore-grain interface, something that can not be done in other approaches such as process-based modeling by Bakke and Øren (1997), where they use an original BSE image of undeformed sandstone to obtain the grain size distribution and finally populate their model with a random spherical grain size distribution and use clay and cement to reach to the approximate angularity of the real grains.

We have used a similar approach to what Blair et al. (1996) used, but they applied that method on images from 2D thin sections of undeformed sandstone, which had simpler pore size distribution compared to deformation bands. Later on Keehm et al. (2004); and White et al. (2006) calculated effective permeability of compaction bands in sandstone through stochastic 3D porous media reconstruction and flow simulation using the Lattice Boltzman method. They used the calculated two-point correlation function of the 2D images (similar to what we calculate) to reconstruct their 3D model. Furthermore, they modeled compaction bands which lack cataclasis. Our research indicates that in order to capture the complex microgeometry of cataclastic deformation bands, we need to take several high magnification images that cover the entire width of the band and use these images to calculate an average specific surface area for the band.

We have resolved the problem of the sensitivity of specific surface area estimation to the resolution of the image (e.g. Keehm et al., 2004) by using high resolution images that provide insight into complex microgeometries. Implementation of image processing methods for deformation bands enables us to map out the variation in porosity and permeability across as well as along tiny deformation bands. Moreover, by applying this method on thin sections of different orientation, we can map out the properties of the band in different orientations (Papers 3 and 4).

Assessing the petrophysical properties of deformation bands

The macroscopic anisotropy across deformation bands and their influence on the petrophysical characteristics of petroleum reservoirs have been addressed before by

among others Antonellini and Aydin (1994), Sigda et al. (1999) and Shipton et al. (2002). The microscopic anisotropy in the properties along a deformation band has been described in Paper 3 of this thesis. Comparison of porosity and permeability estimates from image processing with direct measurements of porosity and permeability from plugs is not straightforward, as the scale of measurement is different. Comparison of our estimated values to lab-measured data shows that the estimated values are always lower than the lab-measured values. We ascribe this difference to the scale limitation (2.54 cm/1 inch) inherent when plug-sized samples are used to measure the properties of millimeter-wide bands.

Our results from image processing show that both porosity and permeability decrease in the studied cataclastic bands compare to the host rock, but the permeability reduction is substantial (up to four orders of magnitude). This is in agreement with lab-measured data (Papers 2, 3) and consistent with the studied cataclastic deformation bands exhibiting more grain crushing than compaction, reducing the grain size and increasing the specific surface area of the pore-grain interface. Hence, the permeability values decrease. In addition, the studied dissolution band (Paper 4) showed up to four orders of magnitude reduction in permeability. This can be also explained by increased specific surface area of the pore-grain interface as a consequence of touching grains.

This study describes new aspects of anisotropy in petrophysical properties such as porosity and permeability induced by deformation bands in the deformed sandstones in microscale. By using our developed image processing method, we have obtained several porosity and permeability measurements for a single band in one thin section, identifying permeability changes up to two orders of magnitude along the band (Paper 4). These changes are related to the variation in microstructure and grain size along the band, as described in the first section of this discussion. We suggest that lateral variations in porosity and permeability documented through image analyses presented in Papers 3 and 4 can explain at least some of the scatter in the porosity and permeability data reported in the literature.

Implications for fluid flow

The effect of deformation bands on fluid flow in a petroleum reservoir depends on the type of deformation band, which is linked to (i) their deformation mechanisms, (ii) their physical properties, and more importantly (iii) the variation of properties such as porosity and permeability across as well as along the bands. Our observations show that

cataclastic deformation bands can reduce absolute permeability values up to four orders of magnitude (Papers 3 and 4). In this sense, they are considered to be important for reservoir management, particularly where they appear in clusters in the damage zones of large faults. On the other hand, rapid spatial variation in properties along bands (Paper 4) implies that deformation bands may rarely be significant pressure barriers and thus probably do not contribute significantly to the sealing capacity of faults (e.g. Harper and Lundin, 1997). In the case of phyllosilicate bands, which are abundant in North Sea petroleum reservoirs, predicting their thickness and continuity is essential for planning oil and gas fields production (Fisher and Knipe, 2001; Hesthammer and Fossen, 2001; Ogilvie and Glover, 2001). Phyllosilicate bands can potentially seal hydrocarbon columns with heights of several hundred metres (Gibson, 1998). During reservoir development, it is important to consider the influence of diagenesis on the petrophysical characteristics of the reservoir, particularly concerning the effect of quartz cement in deep reservoir horizons (more than about 2 km). Finally, the effect of deformation bands on fluid flow in reservoirs depends on their spatial distributions and their abundance, which is beyond the scope of the presented work.

Limitations related to the current study

Research is perhaps always compromised by limitations of some kind, and this research is not an exception. There are limitations inherent both in the instruments applied and in the methods that have been used in this study. The limitations that are related to the individual steps of this research are as follows:

- Constraints imposed by the ring-shear apparatus limited the experiments to (i) a predefined shear surface, and (ii) higher shear displacement than it is required for the formation of deformation bands. Taken together, these make the comparison of experimental shear zones to natural deformation bands less straight forward; this is discussed further in Paper 1.

- The time-consuming segmentation process for grain size analysis and also the image processing for porosity, permeability estimations rely on the quality of the obtained binary image and the level of threshold that a backscatter image is assigned to (Papers 3, 4). A quality check should be done during binarizing images by comparing them to the original BSE images.

- In the Kozney-Carman relation, the constant *c* is considered to be equal to 2 for the pores with circular cross-sections. In order to calculate the formation factor we used an exponential relationship between porosity and formation factor (Archie, 1942). The results could be slightly different if we could measure the formation factors for the studied deformation bands (Paper 3).

Suggestions for future work

- Further investigation is also needed on the initiation and development of deformation bands in a wide range of sandstones with different mineralogy, initial grain size, and porosity.
- The presence of cement at the time of deformation affects the deformation processes and resulting deformation-band properties (e.g. Trent, 1989; Yin and Dvorkin, 1994). The effect of quartz cement on cataclasis and the significance of phyllosilicates on the initiation of quartz cement should be studied further.
- In order to better simulate the natural formation of deformation bands, performing experiments with fluid in the pore spaces (that is, undrained) is recommended. At low confining pressures and in the presence of fluids, minerals such as feldspar are deformed by chemical alteration rather than physical deformation.
- In order to document the detailed microstructure of deformation bands, especially when one is trying to build a 3D geological model, we suggest making thin sections at least in two perpendicular directions.
- High resolution X-ray microtomography can be used to characterize the 3D microgeometry of deformation bands if their resolution is sufficient for capturing the complex microgeometry of cataclastic bands. This type of study may add to our knowledge about deformation bands.
- In the case of slipped deformation bands (Paper 2) more field work is needed to find out whether this kind of band is common in other similar geological settings, and in sandstones with similar petrophysical properties. Besides, understanding the mechanism of formation of slipped bands requires theoretical work, triaxial analogue modeling, and developing their cam-cap model accordingly. The initial material properties, such as grain size and porosity, must be considered in such studies.

References

Agung, M. W., Sassa, K., Fukuoka, H., Wang, G., 2004. Evolution of shear zone structure in undrained ring-shear tests. Landslides 1, 101-112.

Antonellini, M. and Aydin, A., 1994. Effect of faulting on fluid flow in porous sandstones: petrophysical properties, AAPG Bull., 78, 355-377.

Archie, G. E., 1942. The electrical resistivity log as an aid in determining some reservoir characteristics. Trans. Am. Ins. Min. Metall. Pet. Eng., 146, 54-62.

Aydin, A., 1978. Small faults formed as deformation bands in sandstone. Pure and Applied Geophysics 116, 913-930.

Aydin, A. & Johnson, A.M., 1978; Development of faultz as zones of deformation bands and slip surfaces in sandstone. Pure and Applied Geophysics 116, 931-942.

Aydin, A. & Johnson, A. M., 1983. Analysis of faulting in porous sandstones, Journal of Structural Geology 5, 1, 19-31.

Davis, G. H., 1999. Structural geology of the Colorado Plateau region of Southern Utah. Geological Society of America, Special Papres, 342.

Davatzes, N. C., Aydin, A., 2003. Overprinting faulting mechanisms in high porosity sandstones of SE Utah. Journal of Structural Geology, 25, 1795-1813.

Fisher , Q. J. & Knipe, R. J., 2001. The permeability of faults within siliciclastic petroleum reservoirs of the North Sea and Norwegian Continental Shelf. Marine and Petroleum Geology, 18, 1063-1081.

Fossen, H., Schultz, R. A., Mair, K. and Shipton, Z., 2007. Deformation bands in sandstones- a review, Journal of Geological Society, London, 164, 755-769.

Gabrielsen, R. H. & Aarland, R. K., 1990. Characteristics of pre-syn-consolidation structures and tectonic joints and microfaults in fine- to medium-grained sandstones. Rock Joints. Balkema, Amsterdam, 45-50.

Gibson, R. G., 1998. Physical character and fluid-flow properties of sandstone-drived fault zone. Geological Society London, Special Publication 127, 83-97.

Harper, T. R. & Lundin, E. R., 1997. Fault seal analysis: reducing our dependence on empiricism. In: Möller-Pedersen, P. & Koestler, A. G. (eds) Hydrocarbon seals-Importance for Exploration and Production. Norwegian Petroleum Society, Special Publication 7, 149-165.

Hesthammer, J. & Fossen, H., 2001. Structural core analysis from the Gullfaks area, Northern North Sea. Marine and Petroleum Geology 18, 411-439.

Johansen, T. E. S. & Fossen, H. 2008: Internal deformation of fault damage zones in interbedded siliciclastic rocks. Geological Society, London, Special Publicatio, in press.

Ogilvie, S. R., Glover, P. W. J., 2001. The petrophysical properties of deformation bands in relation to their microstructure. Earth and Planetary Science Letters 193, 129-142.

Shipton, Z. K., Evans, J. P., Robeson, K. R., Forster, C: B., Snelgrove, S., 2002. Structural heterogeneity and permeability in eolian sandstone: Implications for subsurface modelling of faults. AAPG Bull. 86, 863-883.

Shipton, Z. K. & Cowie, P. A., 2003. A conceptual model for the origin of fault damage zone structures in high porosity sandstone. Journal of structural Geology, 25, 333-345.

Sigda, J. M., Goodwin, L. B., Mozely, P. S. & Wilson, J. L., 1999. Permeability alteration on small displacement faults in poorly lithified sediments: Rio Grande Rift, Central New Mexico. In: Faults and Subsurface Fluid Flow in the Shallow Crust (edited by Hanberg, W. C., Mozely, P. S., Moore, C. J., Goodwin, L. B.. Geophysical Monograph 113. American Geophysical Union, Washington DC, 51-68.

Trent, B. C., 1989. Numerical simulation of wave propagation through cemented granular material, in AMD-101, Wave Propagation in Granular Media, eds. D. Karamanlidis and R. B. Stout, 9-15.

Yin, H. & Dvorkin, J., 1994. Strenght of cemented grains, Geophysical Research Letters 21, 10, 903-906.

Appendix

```
% This program includes a series of functions that estimate the
%porosity and specific surface area from microscopic images of thin
%sections using statistical physics.

% Note: The authors assumes no responsibility whatsoever for the use of
% the program by other parties, and makes no guarantees, about its
%quality, or any other characteristic.

% Terms of use of this program

% 1) Use of this program by any for-profit commercial organization is
%expressly forbidden unless said organization is a Fault Facies Project
%sponsor.

% 2) A Fault Facies Project sponsor may use this program under the
%terms of the Fault Facies Project Sponsorship agreement.

% 3) A student or employee of a non-profit educational institution may
%use this program subject to the following terms and conditions:
% - this program is for research purposes only.
% - including it or any portion of it, in any software that will be
%resold is expressly forbidden.
% - transferring the program in any form to a commercial firm or any
%other for-profit organization is expressly forbidden.

% (1) The 1st step is reading thin section images into MATLAB.

 I=imread('image file'); %Image matrix has M rows and N columns
%(i=1,2,...M, j=1,2,...N).

 figure, imagesc(I),colormap(gray(256)), grid on;

% By using 'imagesc' function to display the thin section the data is
%scaled to use the full colormap.

figure,imshow(I),grid on; axis on
% imshow displays the grayscale image 'I' without scaling the data.

%=========================================================================
% (2): The 2nd step is to choose part of the image for further work. By
% using 'grid on' and 'axis on' commands in the display functions, we
%can choose the matrix indices of the four corners forming the selected
%area inside the image 'I'.
% The following drawing shows the matrix range for the initial image
'I' %and the cropped image inside the initial image.
%
%        j=1                        j=N
%    i=1  |------------------------|
%         |                        |
%         |  |-----------------|   |
%         |  |                 |   |
%         |  |-----------------|   |
%         |                        |
%   i=M   |------------------------|


% I=I(first row of cropped image: last row of the cropped image, first
%column of cropped image: last column of the cropped image);
```

```
%
==========================================================================
% (3) The 3rd step is to estimate the threshold. There are two ways %to
perform this:
% (3-A) Otsu method (MATLAB built in function)

threshold=graythresh(I);

% graythresh computes a global threshold that can be used to convert
%the image 'I' to a binary image. The resultant value or level is a
%normalized intensity value that lies in the range [0, 1].
% GRAYTHRESH uses Otsu's method, which chooses the threshold to %
%minimize the intraclass variance of the threshold black and
% white pixels.

% (3-B) The second way is to create the data histogram, display it and
%choose the threshold value by visual inspection of the data histogram.
%The numbers of occurrences of the values between 0 and 255 ('counts')
%are displayed. The length of 'counts' is the same length of colormap
%in this case 256.

imhist(I)
[counts,x]=imhist(I);figure, bar(x,counts),

%=========================================================================
% (4) The 4th step is making binary using the estimated threshold
%value.

 bw=im2bw(I, threshold);

% The function is MATLAB build in function that Convert image to binary
%image by thresholding.
% The output binary image BW has values of 1 (white) for all
% pixels in the input image with luminance greater than LEVEL and 0
%(black) for all other pixels.

 figure,imagesc(bw),colormap(gray), grid on % scaled display to
%colormap range
 figure, imshow(bw), grid on, axis on       % Dispaly without scaling

%=========================================================================
% (5) The 5th step is to change the image to a square matrix in case if
%it is not, We select parts of the image that has as less as possible
% broken grains at the edge of the image. This stage is only necessary
%if we calculate the two point correlation function using function
%'xcorr2' (step 8).

     I2=bw(1:m,1:m);

% m is the number of rows and also columns that is selected from the
%image.

  figure, imagesc(I2),colormap(gray), grid on  % scaled display to
%colormap range
  figure, imshow(bw), grid on, axis on       % Dispaly without scaling

%=========================================================================
% (6) The 6th step is reversing the negative image to positive image it
%means pore space from black (0) to white (1). The indicator function
%or phase function or characteristic function is 1 for pores and 0 for
%grains.
```

```
 I3=ones(size(I2)); tes=find(bw); I3(tes)=0; %If we apply the 5th stage
%then here bw will be replaced by I2.
 figure,imagesc(I3),colormap(gray),grid on  % scaled display to
%colormap range
 figure, imshow(I3), grid on, axis on       % Dispaly without scaling

%=========================================================================
% (7) The 7th step is to calculate the one point correlation function
%that is the porosity. The denominator is the product of pixel numbers
% in both directions.


        phi=length(find(I3))/(M*N)
        % MxN is the ranke of I3.

%=========================================================================

% (8) The 8th step is to calculate the two-point correlation function.
%     We have two methods to do this.
% 8-A) First the function we have written called tpcf.m. The function
%  is run as follows:
       S2=tpcf(I3);

% The function detail is given below:
       function s2=tpcf(I3)
% This function calculate the two-point correlation function
%(that is a joint probability function) using the binary image with a
% certain pixel size.

s2(1,1)=length(find(I3))/(length(I3));
s2(1,1);
a=length(I3(:,1));

    b=length(I3(1,:));
    c=a/b;

 for m=3;
   i=1:length(I3(:,1)-m;
  end
    for n=3;
   j=1:length(I3(1,:))-n;
    end
for i=1:length(I3(:,1))-m;
for j=1:length(I3(1,:))-n;

x=I3(i,j);
save x
y=I3(i+m,j+n);
save y
%data(1:m,1:n).test=[x,y]
test=x.*y;
save test
test2=sum(test);
test3=test2/(length(I3));
save test3
%save test
s2(m,n)=sum((I3(i,j)*I3(i+m,j+n))/((a-m)*(b-n)));
 end
```

```
end
       end


% 8-B) The second method is to use the MATLAB built in function called
%  xcorr2.
       test4=xcorr2(I3);
% The only difference is that in the second method we should use two
% more step as follows:
% sub-step 1: Selection of the positive lag of the autocorrelation
function:
       I4=(test4(length(I3(:,1)):end,length(I3(1,:)):end));
       figure,imagesc(I4), grid on  % scaled display to colormap range
       figure, imshow(I4), grid on, axis on     % Dispaly without
%scaling

% sub-step 2: Normalization of the results:
       I4=I4/(length(I3));
       figure, imagesc(I4),grid on % scaled display to colormap range
       figure, imshow(I4), grid on, axis on   % Dispaly without scaling

%=========================================================================
% (9) The 9th step is a main step to convert the calculated two-point
%  correlation function from the Cartesian coordinate system to a
%radial system and then taking average along the certain radiuses.
% The reason for this is to be able to use the spatial correlation data
% derived from 2D images for 3D purposes.
% We have written a function called average.m to do this that is run as
%   follows:

      [test3]=average(I4), figure, plot(test3), grid on
% test3 is a vector that represents the mean values of two point
% correlation function along different radiuses.

function [test3]=average(I4)
% This function is planned to map the two-point correlation function
%from a Cartesian coordinate system to polar coordinate system and then
%taking average along fixed radiuses.
% The input to the function is just the normalized two-point
%correlation function (output of the 8th staep). The output is a vector
%that represents the average values of two-point correlation function
%along the fixed radiuses.

X=1:length(I4(:,1));
Y=1:length(I4(1,:));
test3=[1:length(I4(:,1))/2];
test3=test3';
test3(1)=I4(1,1);
%====================================
[x,y]=meshgrid([1:length(I4(:,1))],[1:length(I4(1,:))]);
for k=2:300;
   l=1:2*k-1;
  v(l)=(pi*l)/(4.*(k));
  XI=k*cos(v);
  YI=k*sin(v);
    s=[XI; YI];
 Z1=interp2(x,y,I4,s(1,2:end-1),s(2,2:end-1)); % 2D interpolation has
been used.
 a=sum(Z1);
 test3(k)=(1/(2.*k+1))*sum(I4(k+1,1)+I4(1,k+1)+a+Z1(1)+Z1(end));
end
```

```
%========================================================================
% (10)to set the scale, and caluculate the slope.

FX(1)=test3(2)-test3(1)
scale=(the scale in main picture)/(number of pixels of the scale bar)
% For example scale bar is 100 micromillimeter and the length of bar in
% pixels are 80 then scale=100/80=1.25

FX(1)=FX(1)./scale

% Now we have the quantity that can be used to calculate specific
%surface area.


     FX(1) = -(specific surface area)/4


     FX(1)=-(specific surface area)/pi
```